

## Article

# Innovative Solutions for Water Treatment: Unveiling the Potential of Polyoxazoline Polymer Activated Carbon Composite for Efficient Elimination of Lead Ions

Abdelfattah Amari <sup>1</sup>, Mohamed Boujelbene <sup>2</sup>, Fatima Moayad Sami <sup>3</sup>, Nouredine Elboughdiri <sup>4,5</sup>, Chandrakant Sonawane <sup>6,\*</sup>, Sujay Raghavendra Naganna <sup>7,\*</sup> and Saad Sh. Sammen <sup>8</sup>

<sup>1</sup> Department of Chemical Engineering, College of Engineering, King Khalid University, Abha 61411, Saudi Arabia; abdefattah.amari@eng.rmu.tn

<sup>2</sup> Industrial Engineering Department, College of Engineering, University of Ha'il, Ha'il 81451, Saudi Arabia; mboujelbene@yahoo.fr

<sup>3</sup> Department of Medical Laboratory Technics, Al-Noor University College, Nineveh 41012, Iraq; fatima.moayad@alnoor.edu.iq

<sup>4</sup> Chemical Engineering Department, College of Engineering, University of Ha'il, Ha'il 81441, Saudi Arabia; ghilaninouri@yahoo.fr

<sup>5</sup> Chemical Engineering Process Department, National School of Engineers Gabes, University of Gabes, Gabes 6029, Tunisia

<sup>6</sup> Symbiosis Institute of Technology, Symbiosis International Deemed University, Pune 412115, India

<sup>7</sup> Department of Civil Engineering, Manipal Institute of Technology Bengaluru, Manipal Academy of Higher Education, Manipal 576104, India

<sup>8</sup> Department of Civil Engineering, College of Engineering, University of Diyala, Baqubah 32001, Iraq; saad123engineer@yahoo.com

\* Correspondence: chandrakant.sonawane@sitpune.edu.in (C.S.); sujay.n@manipal.edu (S.R.N.)



**Citation:** Amari, A.; Boujelbene, M.; Sami, F.M.; Elboughdiri, N.; Sonawane, C.; Naganna, S.R.; Sammen, S.S. Innovative Solutions for Water Treatment: Unveiling the Potential of Polyoxazoline Polymer Activated Carbon Composite for Efficient Elimination of Lead Ions. *Water* **2024**, *16*, 466. <https://doi.org/10.3390/w16030466>

Academic Editor: Amimul Ahsan

Received: 10 December 2023

Revised: 26 January 2024

Accepted: 28 January 2024

Published: 31 January 2024



**Copyright:** © 2024 by the authors. Licensee MDPI, Basel, Switzerland. This article is an open access article distributed under the terms and conditions of the Creative Commons Attribution (CC BY) license (<https://creativecommons.org/licenses/by/4.0/>).

**Abstract:** Heavy metal pollution is a global problem that necessitates the development of innovative and environmentally friendly water treatment technologies. Polyoxazoline polymers, known for their biocompatibility, are explored for lead ion removal in water treatment. Poly 2-Methoxycarbonylpropyl-2-oxazoline is integrated into activated carbon via in situ polymer growth, optimizing loading through live polymerization. This study investigates intricate interactions between lead ions and functional groups, such as amide moieties and ester functionalities, in the resulting polyoxazoline-modified activated carbon composite (POZ-AC). This pioneering research opens avenues for the application of polyoxazoline polymers in water treatment, leveraging their established success in biomedical fields. The removal of lead ions by POZ-ACs followed the Langmuir isotherm and pseudo-second-order kinetic model. The results showed that POZ-AC-20 had excellent adsorption capacity of 365 mg/g, achieved in a relatively short time of 37 min. Furthermore, the adsorbent maintained its performance for seven cycles, demonstrating its high reusability potential. However, the adsorption performance of POZ-ACs after seven adsorption–desorption cycles was gradually decreased due to polymer release into the water media because of the high degree of solubility of polyoxazoline polymers in water. This study provides critical insight into the potential use of polyoxazoline polymers, demonstrating their superior potential in water treatment applications, particularly since it is the first time these polymers have been explored for this purpose. Future research should focus on developing polyoxazoline polymers with less solubility in water while maintaining a high removal performance.

**Keywords:** adsorption; lead ions elimination; polymer networks; water treatment

## 1. Introduction

An uncontaminated environment is essential for the survival of all living organisms and for the preservation of the equilibrium and stability of our ecosystems [1–3]. However, the accumulation of diverse pollutants in industrial waste disposal has resulted in a scarcity of clean water [4,5]. As a consequence, environmental regulations have become increasingly

stringent, and researchers have shifted their focus to developing effective treatments for liquid effluents, safeguarding public health [6–8]. Among these pollutants, heavy metals are a significant concern due to their potent toxicity and profound impact on human well-being [9–11]. Heavy metals are not susceptible to degradation and are refractory, hence necessitating the establishment of permissible limits for their discharge into nature [12].

Heavy metals, including mercury, chromium, cadmium, lead, copper, and cobalt, have been associated with extreme environmental issues [13,14]. Of all the heavy metals, lead (Pb (II)) is of significant importance because of its pronounced toxicity and ability to dissolve in water, which negatively affects the quality of drinking water [15]. The toxic effects of Pb (II) are well documented, causing harm to the human liver, brain, reproductive system and kidneys [16–18]. To address this issue, strict regulations have been put in place, with the European Union countries limiting Pb (II) concentration to 0.01 mg/L and the US Environmental Protection Agency limiting it to 0.05 mg/L [19,20]. Therefore, it is crucial to urgently and effectively eliminate Pb (II) from water bodies to protect human health.

Numerous techniques have been utilized to address heavy-metal-containing waste water, including membrane separation, adsorption, coagulation, flocculation, electrolysis and more [21–24]. Adsorption technologies have been widely adopted owing to their convenient handling of subsequent processes and their acceptable cost range [25,26]. Studies have confirmed that the performance of remediation is predominantly determined by the properties of the adsorbent materials. Recently, a multitude of researchers have devised various adsorbents for the adsorption of heavy metals from water-based environments, incorporating activated carbon, zeolites, metal-organic frameworks (MOFs), and more [27–29]. For example, Mohammadi et al. synthesized amine-modified Cu-MOFs to selectively capture lead ions from real river water. The MOF's porous matrix with high surface area and amine functionalization provided an ideal template for lead removal [30]. In another study, Zheng and colleagues developed ionic liquid-modified polyethersulfone nanofibrous membranes for heavy metal removal, demonstrating the complexation between nitrogen atoms in the imidazolium ring and cadmium ions [31]. Ragheb and colleagues fabricated a magnetic MOF with glutathione attached to its surface, exhibiting excellent heavy metal adsorption facilitated by diverse functional groups, including amine, carboxylate, and sulfur, provided by the glutathione attachment. The dispersion of active sites on the surface of a template material has been widely utilized as an effective approach to the use of the surface area and porous matrix of the template material to capture and host pollutants while utilizing the active sites to their full performance [32].

Polyoxazoline (POZ) is a synthetic polymer with a highly branched, amorphous structure that provides it with unique physicochemical properties [33]. The polymerization of polyoxazoline monomers involves the live cationic ring-opening polymerization of 2-oxazoline monomers [34]. The resulting polymer has a linear chain structure with pendant hydroxyl groups, which can be altered to improve its characteristics and functionality. Due to its excellent hydrophilicity and biocompatibility, it has been extensively explored in biomedical applications, including tissue engineering and drug delivery [35,36]. POZ has a high degree of flexibility and can be easily modified to enhance its affinity for certain purposes. Additionally, the size and shape of POZ particles can be easily controlled through the live polymerization process, making it possible to optimize their performance for specific applications. As an example, researchers have synthesized POZ-modified graphene oxides to enhance the dispersibility of graphene oxide particles in both water and resin [37]. Additionally, polyoxazoline has been effectively incorporated into a silicone matrix to produce amphiphilic coatings [38].

Upon comprehensive examination of the existing literature, it is evident that the potential of polyoxazoline for water treatment applications remains an underexplored domain. Despite acknowledgment of their promise, the full extent of their applicability in this field has yet to be thoroughly investigated. Our study addresses this gap by presenting pioneering work that delves into the utilization of polyoxazoline for water treatment. Specifically, this research focuses on the incorporation of poly 2-Methoxycarbonylpropyl-

2-oxazoline polymers for effective adsorption of lead ions from water into an activated carbon matrix. The live cationic polymerization process of polyoxazolines provides precise control over the polymer loading on the activated carbon by altering the reaction time, as the polymer chain growth is exactly correlated with the quantity of functional groups on the adsorbent. This allows for the incorporation of a range of polymers with varying chain lengths into the activated carbon framework to optimize the polymer loading. This study further investigated the process variables of lead removal and the real-time application of the adsorbents. The synthesized products were characterized using various methods including FTIR, TGA, BET, and SEM.

## 2. Materials and Methods

### 2.1. Materials

The following is the list of chemicals utilized in this study as received: lead nitrate, activated carbon, acetonitrile, piperidine, diethyl ether, methyl p-toluenesulfonate, barium oxide, sodium carbonate, glutaric anhydride, triflic acid, methanol, 2-chloroethylamine hydrochloride, and thionyl chloride. The chemicals were purchased from Sigma–Aldrich company (Burlington, MA, USA) and used without further purification, as they were of analytical grade.

### 2.2. Synthesis Procedure of Poly 2-methoxycarbonylpropyl-2-oxazoline-activated Carbon Composite

The synthesis procedure for 2-Methoxycarbonylpropyl-2-oxazoline monomers was conducted in accordance with a previously reported approach [39]. Typically, the synthesis of monomers involves four steps. Firstly, methanol and glutaric anhydride were reacted to produce monomethyl glutarate. Next, thionyl chloride was used to convert monomethyl glutarate to glutaric acid monomethyl ester chloride. Then, the addition of 2-chloroethylamine hydrochloride led to the formation of C3MestOx amide. The final step was ring-closure of the precursor using anhydrous sodium carbonate. C3MestOx was vacuum-distilled over barium oxide prior to polymerization. The polymerization process was carried out in the presence of triflic acid under nitrogen purging and termination with ethylenediamine. Then, the purification steps included evaporation of the solvent, washing with water, dehydration using  $\text{Na}_2\text{SO}_4$ , and washing with methanol. The product was named POZ. A schematic illustration of the synthesis procedure is presented in Figure 1.

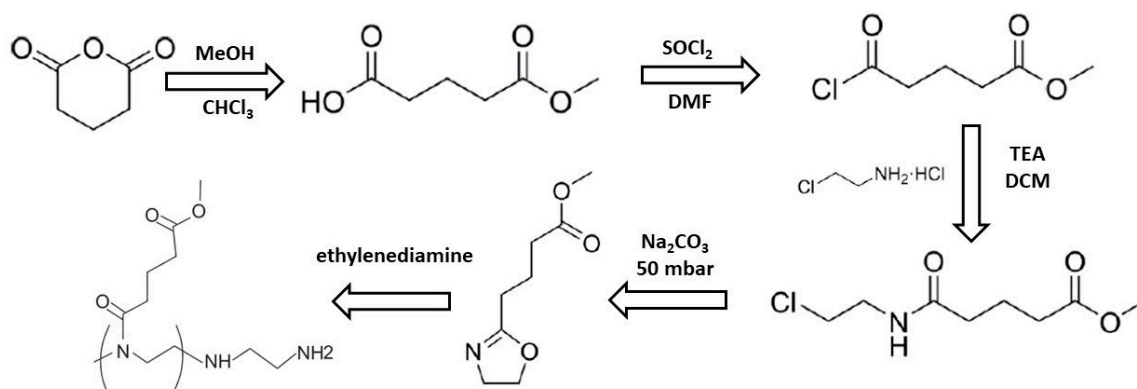


**Figure 1.** Schematic illustration of the synthesis procedure of poly 2-Methoxycarbonylpropyl-2-oxazoline.

To produce POZ-activated carbon composites, firstly, the activated carbons were oven-dried for 4 h at 120 °C. Then, 10 g of dehydrated activated carbon were mixed with 0.7 g of C3MestOx monomers and kept under nitrogen purging for 24 h to ensure that all the monomers were adsorbed within the pore network of the activated carbons. Next, 5 mL of chlorobenzene was introduced into the mixture under nitrogen purging, followed by the introduction of 12  $\mu\text{L}$  of triflic acid as an initiator. After 10 min of purging with

nitrogen under stirring conditions, the mixture was made hot until 90 °C. To optimize the polymer loading, three reaction times were tested: 10, 20, and 30 min. To stop the reaction, ethylenediamine was added to the mixture, which was kept under stirring and a nitrogen atmosphere for 24 h. Finally, the purification process involved the evaporation of the solvent, washing with water, dehydration using Na<sub>2</sub>SO<sub>4</sub>, and washing with methanol. The solvent was then vacuum-evaporated for 12 h. The final products were named POZ-AC-10, POZ-AC-20, and POZ-AC-30, corresponding to the 10 min, 20 min, and 30 min reaction times, respectively.

### 2.3. Instruments

Examining the thermal resilience of adsorbents involved TGA analysis, where temperatures varied between 25 and 950 °C, and the heating rate maintained a constant 10 °C/min. Carried out in an inert atmosphere, the experiment utilized the PerkinElmer Pyris Diamond model as the thermogravimetric analyzer. The nitrogen gas adsorption–desorption patterns were generated using the Micromeritics TriStar II Plus gas adsorption apparatus (Micromeritics, Norcross, GA, USA). Preceding the test, the materials underwent a degassing process at 210 °C for 5 h before being introduced to the adsorption cell, which was maintained at −196 °C for the entire duration of the experiment. FTIR analysis was conducted using the PerkinElmer Spectrum Two spectrometer (PerkinElmer, Buckinghamshire, UK), capturing spectra in the 4000–400 cm<sup>−1</sup> range. The adsorbent pellets, blended with KBr, were employed for this analysis. The Hitachi S-4800 field-emission scanning electron microscope (Hitachi, Tokyo, Japan) was employed for SEM examination. To achieve optimal image resolution, the accelerating voltage was set at 20 kV. Before SEM investigation, a thin conductive layer of gold/palladium alloy was applied to the specimens using a sputter coater (Leica EM ACE600, Wetzlar, Germany). The measurement of lead ions' concentration was performed using a 230 ATS Atomic Absorption Spectrometer (Buck Scientific, East Norwalk, CT, USA). The pH of the solutions was adjusted using an MP511 benchtop pH meter (Apera Instruments, Columbus, OH, USA). Centrifugation was carried out using a benchtop 5810 R Centrifuge model (Eppendorf, Hamburg, Germany). The stirrers used in this study were Stuart digital stirrers (Merck, Rahway, NJ, USA).

### 2.4. Pb (II) Ions' Removal Procedure

A stock solution was formulated through the dissolution of lead nitrate in distilled water to achieve a lead content of 100 mg/L. The effect of lead content was investigated by introducing 250 mg/L of each adsorbent into 50 mL of different solutions containing lead concentrations of 5, 10, 20, 50, 80 and 100 mg/L. These solutions were made by diluting the stock solution. All experiments were carried out in batch mode at 25 °C with a stirring rate of 600 rpm, and the duration of each experiment was set to 24 h to ensure equilibrium.

To study the impact of pH on the lead elimination process, 250 mg/L adsorbent was added to each lead solution, which was then adjusted to the desired pH level (pH range of 2–8 and lead content of 50 mg/L) by adding either HCl or NaOH. The contact time between adsorbent and adsorbate particles was also examined by measuring lead removal over specific time intervals. For this purpose, 250 mg/L adsorbent was combined with a lead solution with a lead content of 100 mg/L, and small samples were collected within a time range of 1–180 min.

Following each adsorption process, the adsorbent was extracted via centrifugation from the mixture, and the supernatant was analyzed further. The final concentration of lead in each supernatant was determined by using an atomic absorption spectroscopy device. The percentage of lead removal was then calculated for each condition, and the optimal conditions (highest lead removal percentage) were identified.

To recover the adsorbent, it was rinsed with distilled water and then eluted with a solution of 1M NaOH to remove the adsorbed lead ions. The adsorbent was washed and eluted multiple times until the eluent no longer contained lead ions. Finally, the adsorbent was dried for reuse.

The lead elimination capacity onto POZ-ACs was measured by the following equations:

$$Q_e(\text{mg/g}) = \frac{(C_i - C_e) \times v}{m} \quad (1)$$

$$\text{Lead removal percentage} = \frac{(C_i - C_e) \times 100}{C_i} \quad (2)$$

Here,  $m$  indicates the mass (in grams) of POZ-ACs utilized for the lead elimination process,  $v$  denotes the volume of the samples (L), and  $C_i$  ( $\text{mg L}^{-1}$ ) denotes the initial lead content, while  $C_e$  ( $\text{mg L}^{-1}$ ) represents the lead content after the elimination process.

### 3. Results and Discussion

#### 3.1. Synthesis and Characterization of Adsorbents

The FTIR spectra for both polyoxazoline polymer and POZ-ACs are shown in Figure 2. In the FTIR spectra of POZ polymer, the absorption band at  $2938 \text{ cm}^{-1}$  corresponds to the bending vibration of the C–H bond [40,41]. The absorption band at  $3280 \text{ cm}^{-1}$  corresponds to the bending vibration of the N–H [42,43]. However, the band at  $1720 \text{ cm}^{-1}$  can be attributed to the bending vibration of the C=O bond in the ester group and band at  $1620 \text{ cm}^{-1}$  can be corresponded to the bending vibration of the C=O in the pendant group of the polymer [44]. The high level of intensity observed in the  $1620 \text{ cm}^{-1}$  band indicates the existence of a high concentration of carbonyl groups in the polymer structure. The absorption band is attributed to the bending vibration of the N–H bond at  $1552 \text{ cm}^{-1}$ , while the band at  $1422 \text{ cm}^{-1}$  is attributed to the bending vibration of the C–H bond [44]. The band at  $1252 \text{ cm}^{-1}$  can be corresponded to the bending vibration of the C–N bond. When activated carbon was loaded with polyoxazoline polymer, changes in the FTIR spectrum were observed (Figure 2). For the C=O bending vibration of the carbonyl group at  $1620 \text{ cm}^{-1}$ , the peak in the polymer backbone remains relatively unchanged, indicating that the improvement did not significantly alter the polymer structure. However, novel peaks emerge in the spectral analysis of the POZ-ACs. A broad peak at  $3420 \text{ cm}^{-1}$  can be corresponded to O–H bending vibrations. The peak at  $1635 \text{ cm}^{-1}$  can be corresponded to the C=C bending vibration of the aromatic ring in the activated carbon. Finally, at around  $1200 \text{ cm}^{-1}$ , the weak peak corresponds to the C–O stretching vibration of carboxylic acid groups [45]. Other peaks related to the polymer structure also remained relatively unchanged and are visible in the spectrum of AC-POZs. These peaks imply the successful loading of activated carbon with polyoxazoline polymers.

The isotherms captured from the  $\text{N}_2$  adsorption–desorption experiments carried out over POZ, AC, and POZ-AC samples are depicted in Figure 3. It is noteworthy that all AC and POZ-AC samples exhibit a type IV isotherm hysteresis loop with an H1, signifying the existence of mesoporous and cylindrical or slit-like pores. The specific surface area (SSA) and total pore volume (TPV) was determined using the BET and BJH techniques. As anticipated, pure POZ displays a meager SSA and TPV owing to its inherent polymer nature, with a surface area of only  $0.33 \text{ m}^2/\text{g}$  and a TPV of  $0.002 \text{ cm}^3/\text{g}$ . A comparison of SSA and TPV values for AC and POZ-ACs is presented in Table 1. Notably, polymer modification reduces the SSA and TPV values for AC. Since the polymerization process mainly occurs inside the pores, the polymer covers the pore walls and leads to a reduction in SSA and TPV. Furthermore, an increase in polymer loading reduces these parameters. Upon comparative analysis of POZ-AC-30 and AC, a substantial decrease in SSA and TPV was detected for POZ-AC-30, with values declining from  $443.8$  to  $311.2 \text{ m}^2/\text{g}$  and from  $0.97$  to  $0.34 \text{ cm}^3/\text{g}$ , respectively. This observation can be corresponded to the growth of polymer chains during the 30 min reaction period, which led to the occupation of the majority of the pore spaces. The BJH method was also utilized to assess the pore size distribution (PSD) of the samples. The results show that the activated carbon has a bimodal PSD with pore sizes centered at approximately 5 nm and 20 nm. In contrast, the POZ-AC samples exhibit a bimodal PSD centered around 16 nm and 4 nm after polymer loading. It

is observed that increasing polymer loading results in a reduction in the pore volume of larger pores. Given the confined space of small pores, polymerization mainly occurs inside larger pores or on the outer surface of AC.

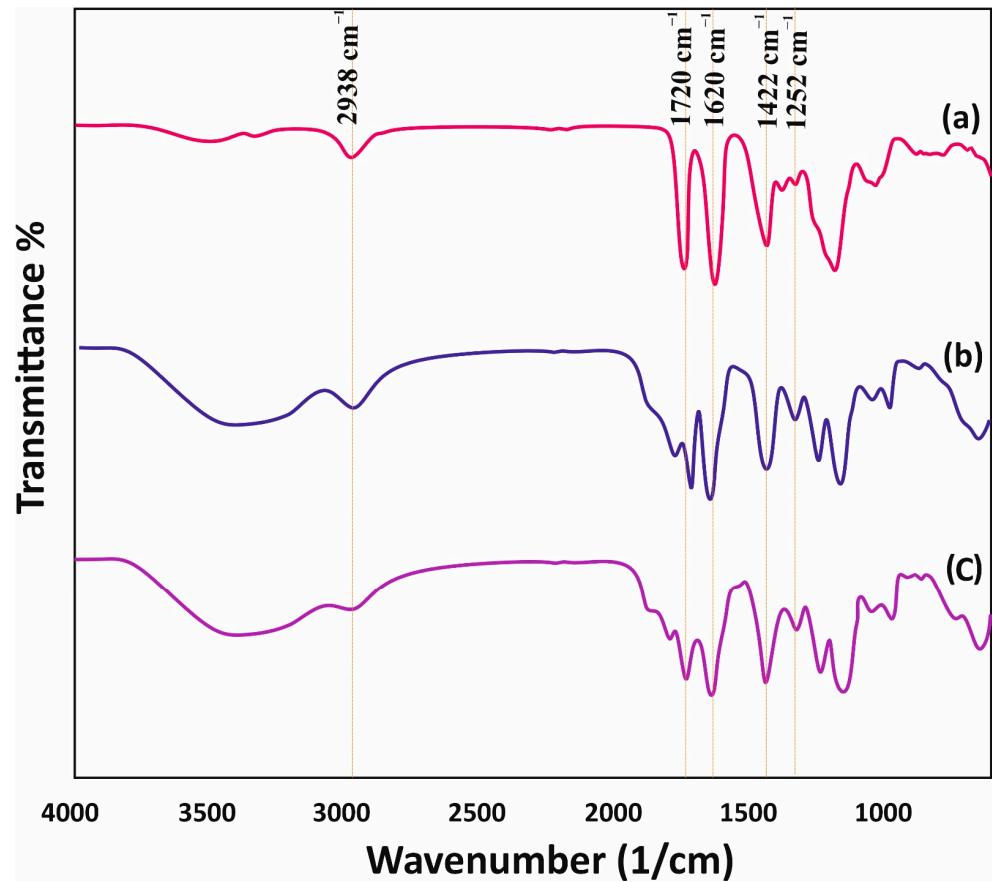


Figure 2. FTIR spectra of (a) 2-Methoxycarbonylpropyl-2-oxazoline, (b) POZ-AC-20, (c) POZ-AC-20 after adsorption.

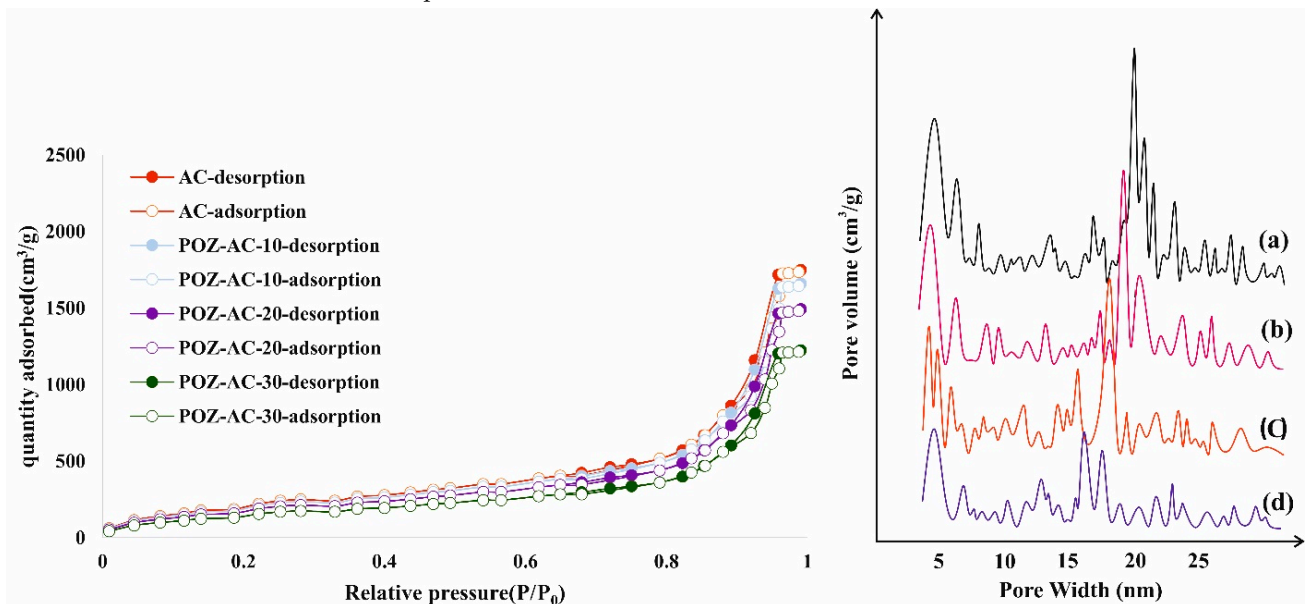


Figure 3. (left) N<sub>2</sub> adsorption–desorption isotherms, (right) pore size distribution of (a) activated carbon, (b) POZ-AC-10, (c) POZ-AC-20, and (d) POZ-AC-30.

**Table 1.** Textural properties of activated carbon and POZ-ACs.

Material	S <sub>BET</sub> (m <sup>2</sup> /g)	Total Pore Volume (cm <sup>3</sup> /g)
Activated carbon	443.80	0.970
POZ-AC-10	420.90	0.811
POZ-AC-20	378.40	0.652
POZ-AC-30	311.20	0.341

The TGA analysis of both activated carbon and POZ-ACs is presented in Figure 4. The thermal degradation behavior of AC was observed in two distinct stages. The initial weight loss of approximately 3% was ascribed to the removal of adsorbed moisture at temperatures below 200 °C. Subsequently, a major weight loss of around 60% between 400 and 700 °C occurred, indicating the decomposition and volatilization of the AC structure. On the other hand, the POZ-ACs exhibited a different two-stage weight loss profile. The first stage, observed at around 320 °C, can be ascribed to the breakdown of oxygen-containing functional groups and the breakdown of the polymer structure, releasing carbon dioxide, carbon monoxide, and steam [37]. The second weight loss step, observed at temperatures above 400 °C, was associated with the degradation of the AC structure. These results suggest that the modification of activated carbon with polymers alters the thermal degradation behavior of AC.

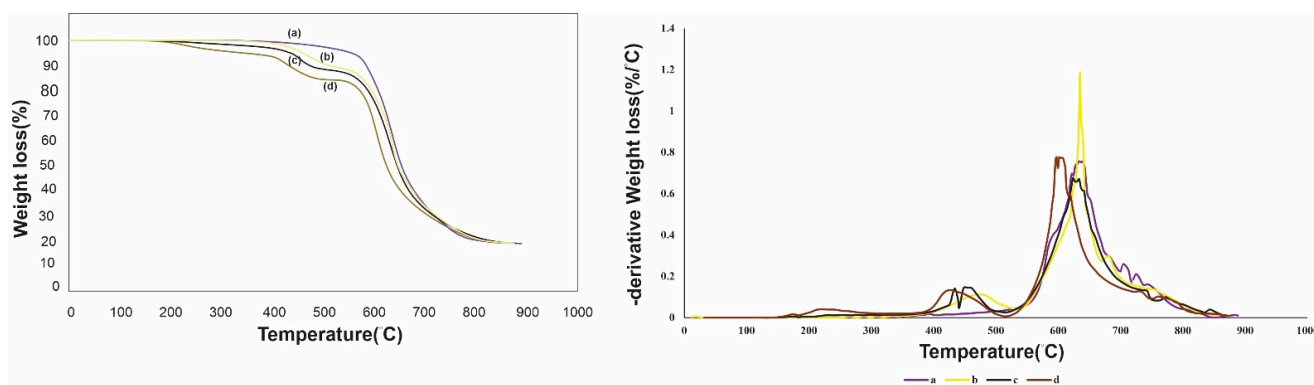
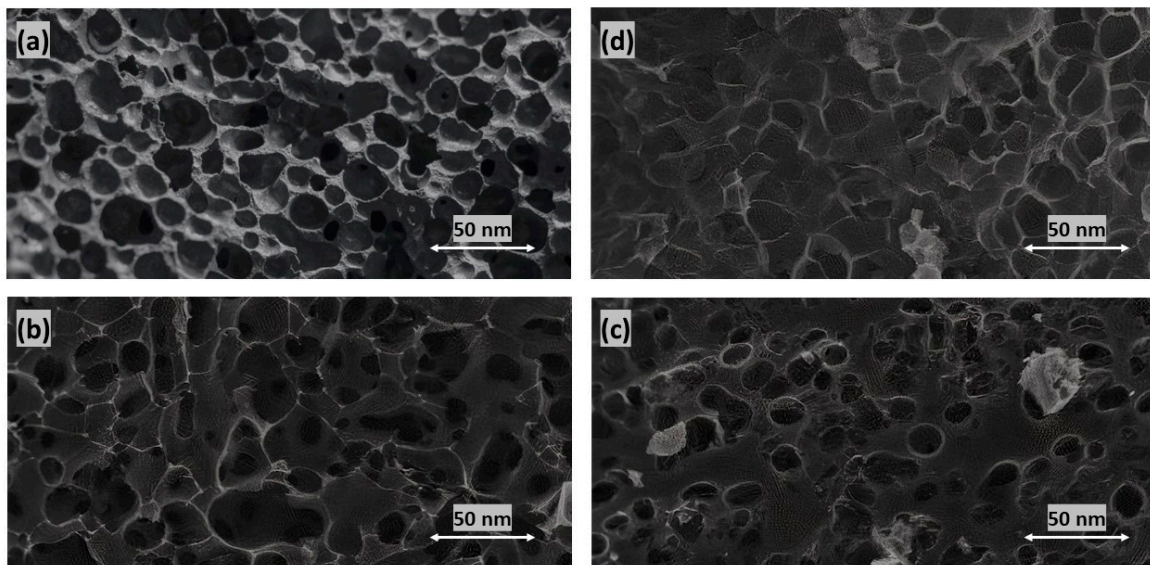
**Figure 4.** TGA analysis of (a) activated carbon, (b) POZ-AC-10, (c) POZ-AC-20, and (d) POZ-AC-30.

Figure 5 shows the SEM images of the activated carbon and POZ-ACs samples. The SEM image of the activated carbon revealed a slit-like pore network, which was consistent with the N<sub>2</sub> adsorption–desorption isotherms. The image also showed a uniform pore network. Similarly, the SEM images of the POZ-ACs displayed uniform pore networks, indicating that the polymer loading did not significantly alter the porous framework of the activated carbon. However, it was evident that the polymer coverage of the pore walls increased with the length of polymer chains in POZ-AC-10, POZ-AC-20 and POZ-AC-30, respectively. These observations are consistent with the results of the BET analysis, which showed a reduction in surface area and pore volume as the polymer loading increased. The increase in polymer coverage on the pore walls of the POZ-ACs likely contributed to this reduction. These findings highlight the impact of polymer modification on the morphology and porosity of the POZ-ACs, which affects their performance in lead removal application.



**Figure 5.** SEM images of (a) activated carbon, (b) POZ-AC-10, (c) POZ-AC-20, (d) POZ-AC-30.

### 3.2. Investigation of the Adsorbent Dosage on Lead Ions' Removal Performance

From an economic standpoint, the quantity of adsorbent utilized in the process holds significant importance. In large-scale applications, the primary determinant of the economic feasibility of the entire process is often the cost of the adsorbent. Consequently, optimizing the dosage of adsorbent plays a crucial role in cost reduction. To achieve this goal, various amounts of adsorbent were introduced to a 50 mL solution containing 5 mg/L lead, maintaining a contact time of 24 h to reach equilibrium. The results depicting the impact of adsorbent dosage are presented in Figure 6. The increase in adsorbent quantity led to an improved lead uptake, attributed to the heightened availability of adsorption sites. However, it was noted that beyond a certain threshold, there was only a marginal increase in lead uptake with larger adsorbent amounts. As a result, an adsorbent dose of 250 mg/L was identified as the optimal amount. This optimum adsorbent dose was subsequently employed for the remainder of this study.

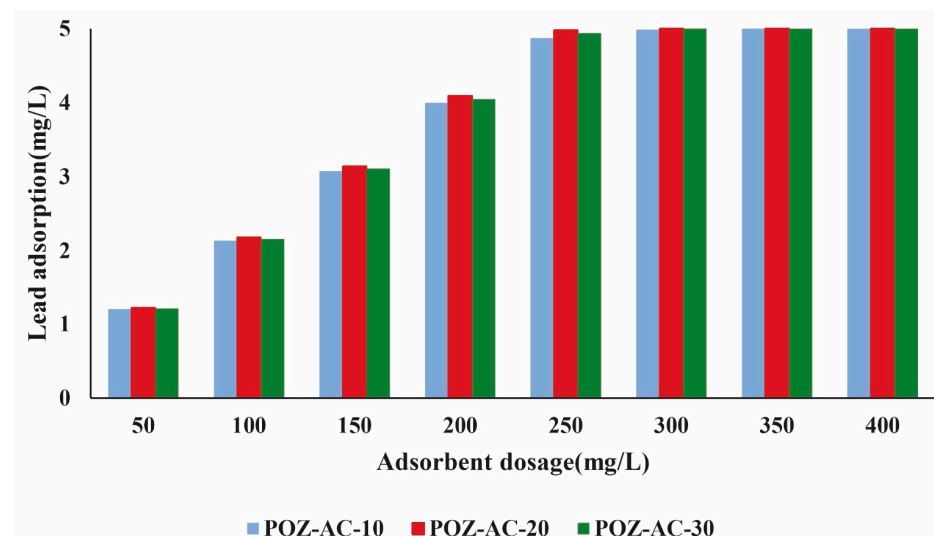


**Figure 6.** The effect of POZ-ACs dosage on lead adsorption.

### 3.3. Investigation of Lead Ions' Removal Using Isotherm Analysis

This section investigates the adsorption of lead ions onto POZ-AC adsorbents using isothermal analysis over metal concentration range of 5 mg/L to 100 mg/L. To this end,

the experimental data underwent analysis through the Langmuir and Freundlich isotherm models. The equations for isothermal models are as follows:

$$\frac{1}{q_e} = \frac{1}{(C_e \times q_m \times K_l)} + \frac{1}{q_m} \quad (3)$$

$$\text{Log}q_e = \text{Log}K_f + \frac{1}{n} \times \text{Log}C_e \quad (4)$$

Here,  $K_l$ ,  $K_f$ ,  $C_e$ , and  $q_e$  represent Langmuir and Freundlich equilibrium constants, equilibrium concentration of lead ions, and lead ions' removal capacity after achieving equilibrium, respectively.  $q_m$  and  $n$  denote the largest theoretical lead ions' adsorption capacity and Freundlich adsorption coefficient, respectively. The high  $R^2$  values obtained from the Langmuir isotherm imply that the adsorption of lead ions onto POZ-ACs was accurately described by this model. Specifically, the corresponding  $R^2$  values for lead removal using POZ-AC-10, POZ-AC-20, and POZ-AC-30 were 0.989, 0.997, and 0.994, respectively. The Langmuir isotherm describes the adsorption on a surface characterized by a limited number of adsorption sites, which are equally available for adsorption. This model generally exhibits less affinity than the Freundlich isotherm, indicating that less energy is required to transfer the particles of the adsorbate originating from the bulk solution to the adsorption sites. The participation of different functional groups in the adsorption process of lead ions as active sites onto POZ-ACs, as illustrated in the FTIR analysis, confirms the provision of an additional pathway for the adsorbate to be adsorbed onto the surface of the POZ-ACs, thus reducing the amount of energy required to overcome the barriers. As shown in Figure 7 and Table 2, the Langmuir model yielded the largest lead removal capacities of 240.7, 365.5, and 112.3 mg/g for POZ-AC-10, POZ-AC-20, and POZ-AC-30, respectively. Figure 8 compares the impact of initial metal concentration on the adsorption performance of POZ-AC-10, POZ-AC-20, and POZ-AC-30. According to this figure, the adsorption capacities of POZ-ACs obtained from experimental data closely match those of theoretical values obtained from isotherm models. A comparison between POZ-AC-10 and POZ-AC-20 indicates that the rise in adsorption capacity can be attributed to the enlargement of polymer chains in POZ-AC-20, which provides additional active adsorption sites. However, when comparing POZ-AC-20 and POZ-AC-30, the reduction in adsorption capacity is attributed to the steric hindrance of the long polymer chains in POZ-AC-30, which cover the majority of pore volumes and pore walls. Table 3 presents an overview of recently developed adsorbents for lead ions' removal from aqueous environments. In comparison to previously developed adsorbents, POZ-AC-20 showcased remarkable efficiency in eliminating lead ions from water. For example,  $\text{NH}_2\text{-SiO}_2\text{@Cu-MOF}$ , despite possessing a specific surface area of  $1111 \text{ m}^2/\text{g}$  and a highly porous structure, only exhibited a lead ion adsorption capacity of  $166.67 \text{ mg/g}$  [30]. Similarly,  $\text{Ni}_{0.6}\text{Fe}_{2.4}\text{O}_4\text{-UiO-66-PEI}$  had a lead adsorption capacity of  $273.2 \text{ mg/g}$ , which was lower than that of POZ-AC-20 [46]. The application of poly 2-Methoxycarbonylpropyl-2-oxazoline polymers as adsorption sites for heavy metal removal is a promising avenue for future research. It is anticipated that a better dispersion of these polymers in porous media could significantly enhance their adsorption capacity.

**Table 2.** Parameters fitted for the Langmuir and Freundlich isotherms.

	Langmuir			Freundlich		
	$q_m$ (mg g <sup>-1</sup> )	$K_l$ (L mg <sup>-1</sup> )	$R^2$	$n$	$K_f$ (mg g <sup>-1</sup> )	$R^2$
POZ-AC-10	240.7	0.7	0.989	2.44	67.17	0.901
POZ-AC-20	365.5	2.5	0.997	2.1	173.38	0.913
POZ-AC-30	112.3	0.35	0.994	4.77	53.32	0.829

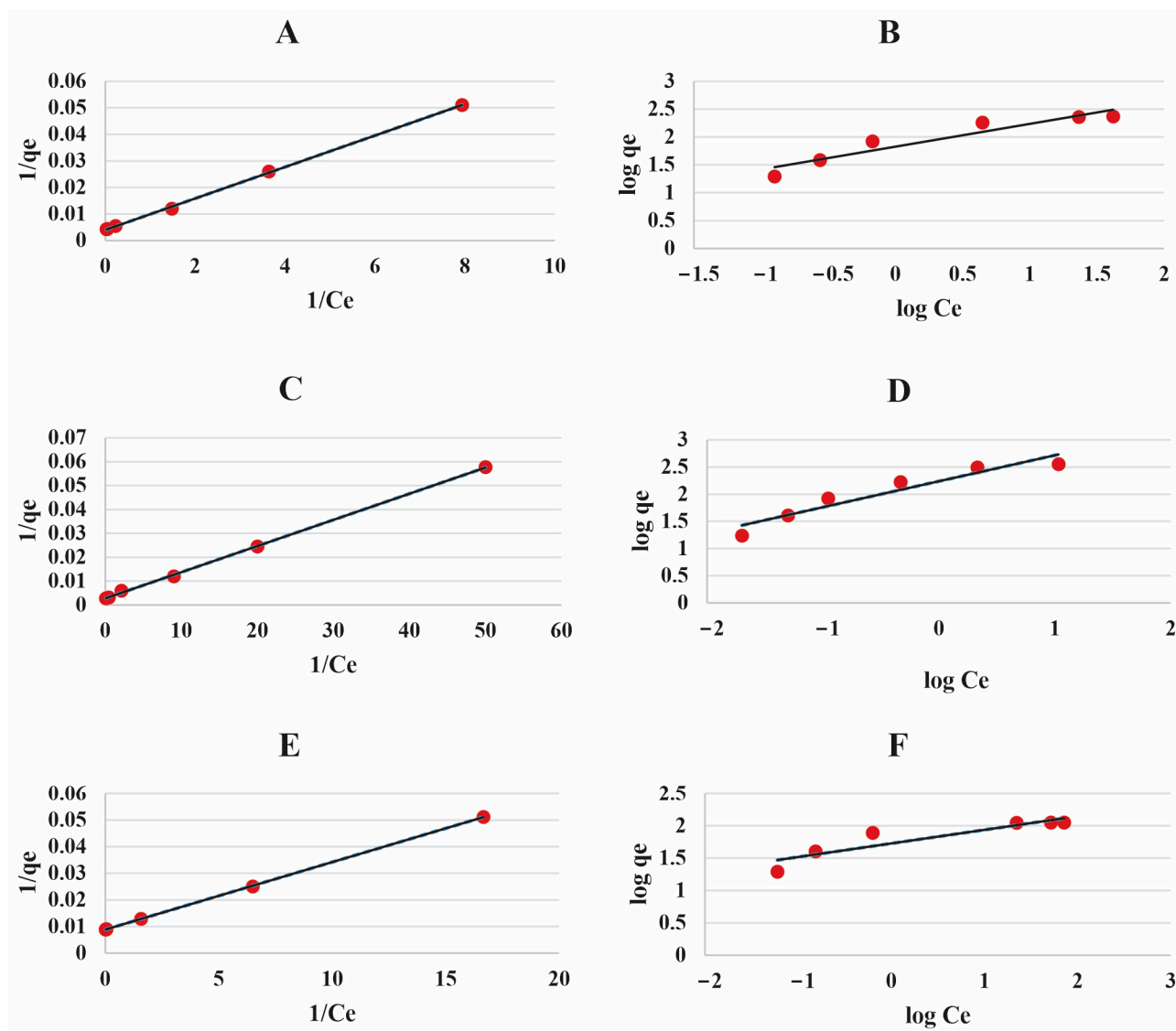


**Figure 7.** (A) Langmuir isotherm of POZ-AC-10, (B) Freundlich isotherm of POZ-AC-10, (C) Langmuir isotherm of POZ-AC-20, (D) Freundlich isotherm of POZ-AC-20, (E) Langmuir isotherm of POZ-AC-30, (F) Freundlich isotherm of POZ-AC-30.

**Table 3.** Comparison of different MOFs for lead ion removal.

Adsorbents	Lead Ion Adsorption Capacity (mg/g)	References
$\text{NH}_2\text{-SiO}_2\text{@Cu-MOF}$	166.7	[30]
thiol-functionalized $[\text{Cu}_4\text{O}(\text{BDC})_n]$	38.7	[47]
UiO-66-NHC(S)NHMe	49	[48]
$\text{Ni}_{0.6}\text{Fe}_{2.4}\text{O}_4\text{-UiO-66-PEI}$	273.2	[49]
MIL-101	15.8	[50]
UiO-66-NDC/GO	254.45	[51]
Co-Al-LDH@CS/ $\text{Fe}_3\text{O}_4$	558.84	[52]
LDH/MOF NC	301.4	[53]
POZ-AC-20	365	Present study

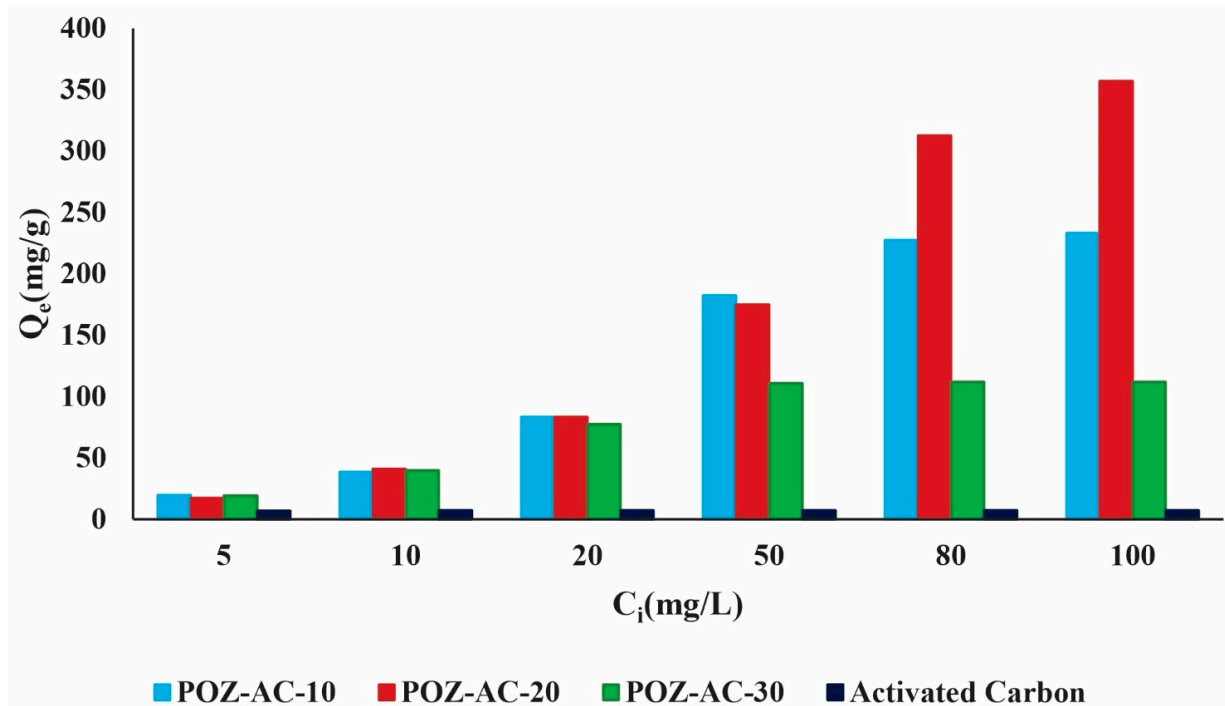


**Figure 8.** Effect of initial metal ion concentration on adsorption capacities of adsorbents.

### 3.4. Investigation of the Kinetic Behavior

In order to confirm the enhancement in the efficiency of lead ion adsorption onto POZ-ACs, a set of adsorption experiments were conducted at specific intervals. The obtained data were subsequently analyzed through the application of both pseudo-first- and pseudo-second-order kinetic models to determine the most effective approach. The corresponding equations for these models are as follows:

$$\ln(q_m - q_t) = \ln q_m - K_1 \times t \quad (5)$$

$$\frac{t}{q_t} = \frac{1}{K_2 \times q_m^2} + \frac{t}{q_m} \quad (6)$$

The parameters in these equations are  $q_t$ ,  $q_m$ ,  $K_1$ , and  $K_2$ , which represent lead ion adsorption capacity after time  $t$ , theoretical adsorption capacity, and constant kinetic model parameters, respectively. This study revealed that the attainment of adsorption equilibrium occurred in a significantly short duration across all adsorbents. According to Figures 9 and 10, and Table 4, which show the effect of equilibrium time on the adsorption capacities of POZ-ACs, the sequence of lead ion adsorption rates was recorded as 25 min, 32 min, and 47 min for POZ-AC-30, POZ-AC-20, and POZ-AC-10, respectively. The increased number of active sites from long polymer chains in POZ-AC-30 facilitated faster lead ions' adsorption. The kinetics of lead ions' adsorption by POZ-ACs were suitably described by the pseudo-second-order model, implying that the rate-controlling factor was chemical adsorption. This observation provides further evidence of the strong affinity between POZ-ACs and lead ions, which could be corresponded on the surface of the adsorbent to the abundance of active sites. In addition, the intra-particle diffusion model was employed for the analysis of the kinetic data, as illustrated in Figure 11. In accordance with the intra-particle kinetic model, a linear graph intersecting the origin signifies that the exclusive limiting factor is intra-particle diffusion. Conversely, a deviation from the origin in the graph suggests the involvement of supplementary processes affecting the process rate, indicating that intra-particle diffusion alone is not responsible for the rate [54,55]. Figure 11 visually represents this departure from the origin.

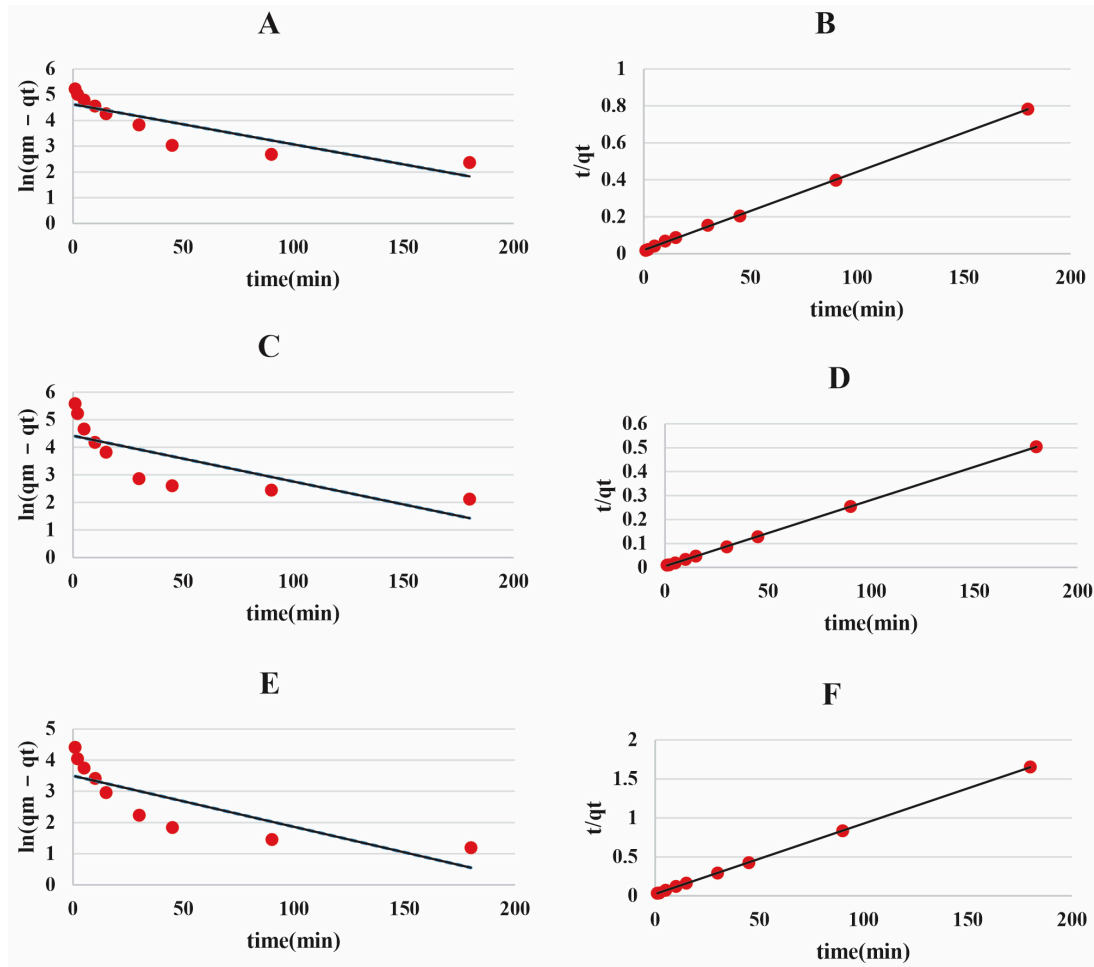


**Figure 9.** (A) Pseudo-first-order model of POZ-AC-10, (B) pseudo-second-order model of POZ-AC-10, (C) pseudo-first-order model of POZ-AC-20, (D) pseudo-second-order model of POZ-AC-20, (E) pseudo-first-order model of POZ-AC-30, (F) pseudo-second-order model of POZ-AC-30.

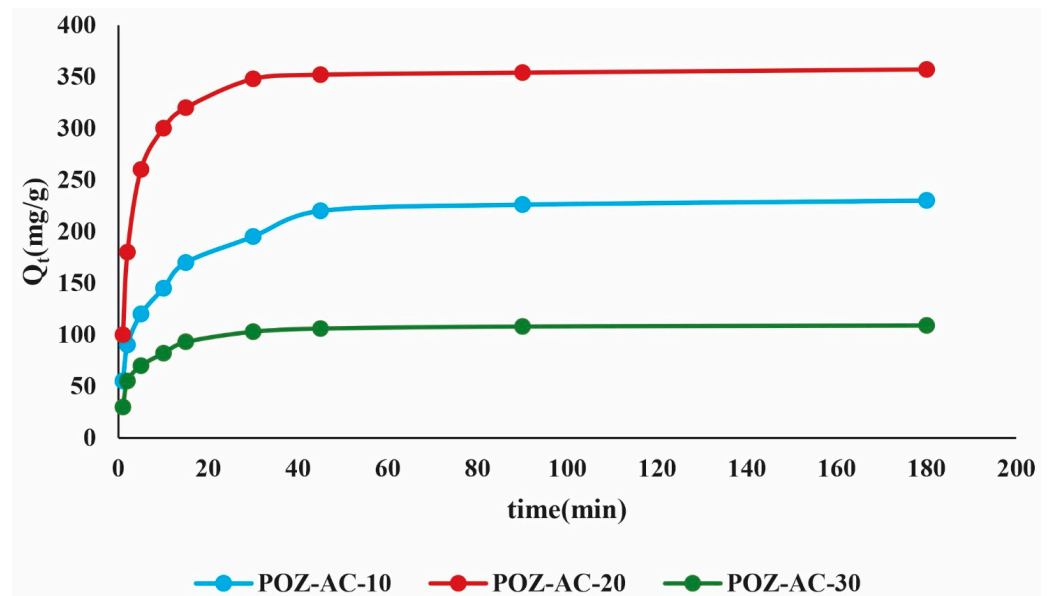


**Figure 10.** Effect of equilibrium time on adsorption performance of POZ-ACs.

Table 4. Parameters fitted for the pseudo-first-order and pseudo-second-order kinetic models.

Materials	Pseudo-First-Order				Pseudo-Second-Order		
	Experimental $q_m$ (mg g <sup>-1</sup> )	Theoretical $q_m$ (mg g <sup>-1</sup> )	$K_1$ (1/min)	$R^2$	Theoretical $q_m$ (mg g <sup>-1</sup> )	$K_2$ (g/mg·min)	$R^2$
POZ-AC-10	233.1	102.15	0.0155	0.7589	238.09	0.0009	0.9995
POZ-AC-20	357.19	83	0.0166	0.592	357.14	0.0015	0.9999
POZ-AC-30	111.9	33.11	0.0164	0.6759	111.11	0.0034	0.9999

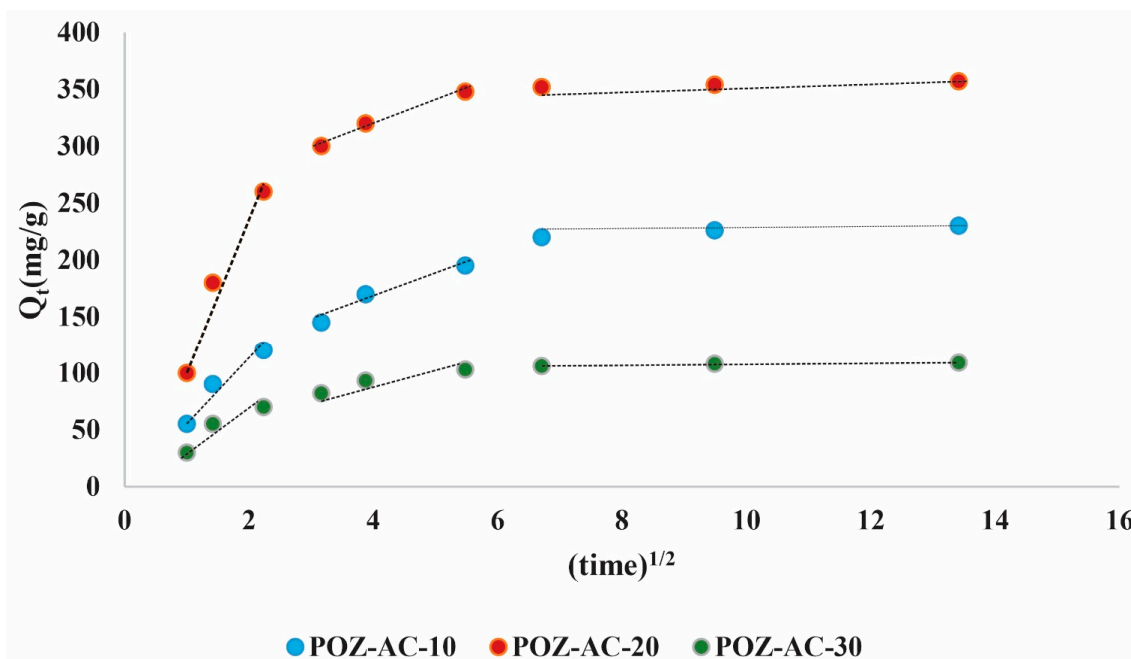
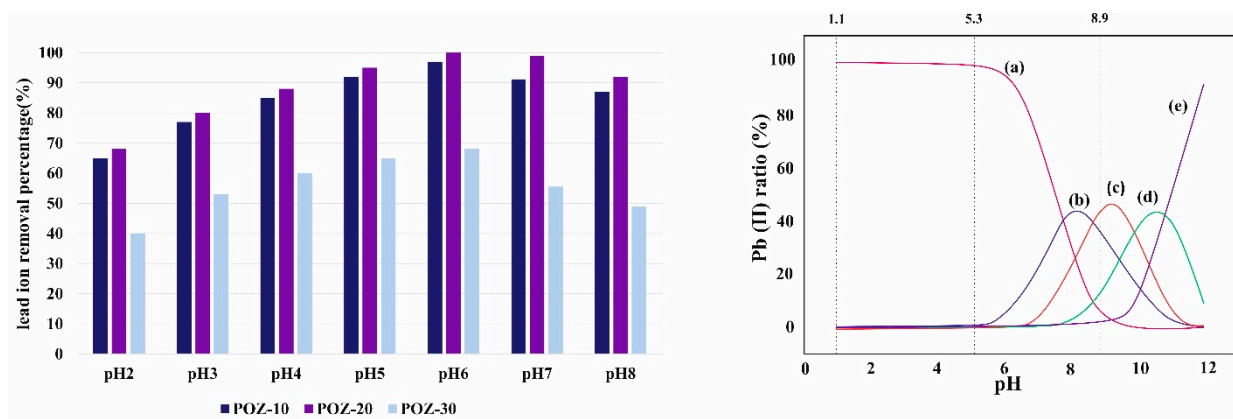


Figure 11. Intra-particle diffusion model for kinetic data of lead adsorption onto POZ-ACs.

### 3.5. Investigation of the pH Impact on Lead Ions' Removal Performance

The speciation of lead ions in different pH values was analyzed, as illustrated in Figure 12. The results demonstrated that the prevalent species of lead ions within the pH range of 2 to 6 was Pb<sup>2+</sup> ion. At pH 2, the percentage of Pb<sup>2+</sup> ion was 99.99%, decreasing to 98.31% at pH 6. At higher pH values (7 to 12), the dominant species changed to Pb(OH)<sup>+</sup>, Pb(OH)<sub>2</sub>, and Pb(OH)<sup>3-</sup>. The percentage of Pb<sup>2+</sup> ion decreased significantly to 65.26% at pH 7, further decreasing to 0.26% at pH 12. To study the impact of pH on the removal of lead onto POZ-ACs, each adsorbent (250 mg/L) was added to a lead solution, which was then adjusted to the desired pH level (pH range of 2–8) by adding either HCl or NaOH. This investigation was only viable in the pH range of 2–8 due lead ions precipitate at pH values higher than 8, preventing experimental monitoring. The research revealed that pH exerted a substantial impact on the uptake of lead ions by POZ-ACs, with the highest removal efficiency being observed at pH 6. According to the point of zero charge calculations of the adsorbents, the surface charge of POZ-ACs at pH 6 was near zero, and the majority of the lead ions were in the adsorbable form of Pb<sup>2+</sup> ion, resulting in optimal attraction between the positively charged lead ions and the negatively charged adsorption sites. The removal efficiency decreased at lower pH values due to the competitive interaction between hydrogen ions and lead ions for the available adsorption sites. Conversely, at alkaline pH, the surface of POZ-ACs became negatively charged, and the dominant lead species changed from Pb<sup>2+</sup> to Pb(OH)<sup>+</sup>, Pb(OH)<sub>2</sub>, and Pb(OH)<sup>3-</sup>, which reduced the attraction between the lead ions and the adsorption sites. These findings suggest that the adsorption of lead ions onto POZ-ACs is significantly influenced by the pH level of the solution.



**Figure 12.** (left) pH effect on the lead ions' adsorption performance, (right) lead ions' speciation at different pH values (a)  $\text{Pb}^{2+}$ , (b)  $\text{PbOH}^+$ , (c)  $\text{Pb}_3(\text{OH})_4^{2+}$ , (d)  $\text{Pb}(\text{OH})_2$ , (e)  $\text{Pb}(\text{OH})_3^-$ .

### 3.6. Adsorption Mechanism

The FTIR spectra after the metal ion adsorption process is provided in Figure 2 (c) to study the mechanism of lead ion removal by POZ-ACs and the involved moieties. Our analysis revealed that the peaks at  $1620$  and  $1552\text{ cm}^{-1}$ , which correspond to the bending vibration of the carbonyl group and the bending vibration of N–H group, slightly decreased, indicating the interaction between the amide group and the lead ions. Additionally, the peak in the ester group at  $1720\text{ cm}^{-1}$  attributed to the stretching vibration of the C=O bond decreased and shifted slightly, demonstrating the involvement of ester groups in the adsorption process. Furthermore, the peak at approximately  $500\text{ cm}^{-1}$ , which is attributed to the bending vibration of the metal–ligand bond, appeared after the removal of lead ions, indicating the formation of lead–polymer coordination bonds. We also observed that the peak at  $1635\text{ cm}^{-1}$ , which corresponds to the C=C bending vibration of the aromatic moiety in the activated carbon, slightly changed, suggesting possible weak electrostatic interactions between the aromatic moieties of activated carbon and lead ions. Overall, the removal process of lead ions by POZ-ACs involves complex interactions of lead ions and specific functional groups. A schematic illustration of the adsorption mechanism is presented in Figure 13.

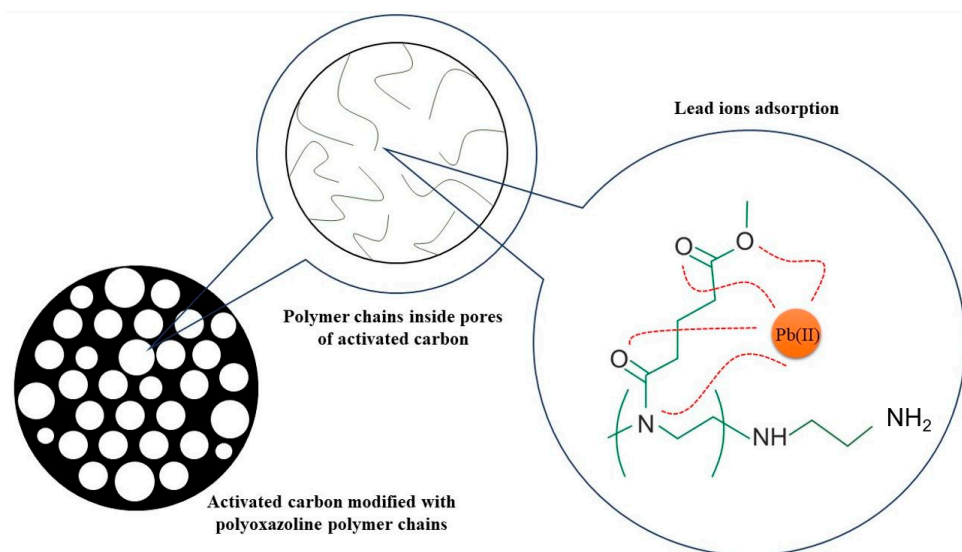


**Figure 13.** Mechanism of lead ions' adsorption via POZ-ACs.

### 3.7. Investigation of Adsorbent Reusability

The reusability of an adsorbent is a critical consideration when evaluating its potential for practical applications. In this study, the reusability of POZ-AC adsorbents was examined through multiple adsorption–desorption cycles. The results showed that even after seven repeated uses, the POZ-ACs maintained a high level of adsorption capacity, albeit with a gradual decline. This decline in performance can be attributed to the high degree of solubility of polyoxazoline polymers, which are released into the liquid during the adsorption–desorption process, thereby reducing the quantity of active sites accessible for lead adsorption. It was observed that the performance decrease followed the sequence of POZ-AC-10 > POZ-AC-20 > POZ-AC-30, consistent with the degree of solubility of polyoxazoline polymers (Figure 14). Shorter polyoxazoline polymer chains have a greater solubility in water, leading to a more significant reduction in polymer release and adsorption performance. While polyoxazoline polymers are considered safe for use in water treatment due to their biocompatibility and non-toxic nature, it is crucial to prevent their leaching into water media to maintain the cost effectiveness of the treatment process. Therefore, future research efforts could focus on developing polyoxazoline polymers with reduced solubility in water while maintaining a high lead removal performance. Such research would be valuable in expanding the practical applications of POZ-ACs as efficient and sustainable adsorbents for heavy metal removal.

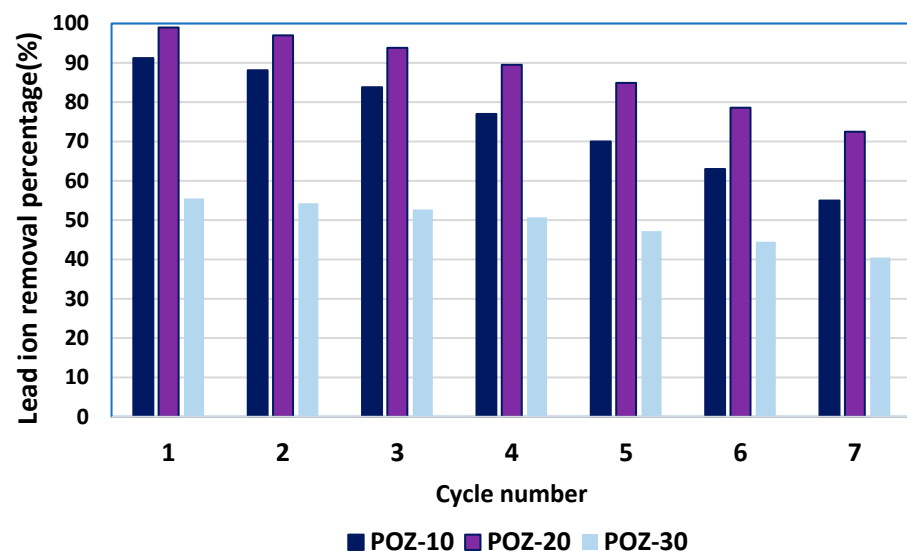


Figure 14. Recovery study of POZ-ACs for lead ions' adsorption process.

## 4. Conclusions

In conclusion, the current study explored the potential of polyoxazoline polymers in water treatment for the first time. The live polymerization mechanism of poly 2-Methoxycarbonylpropyl-2-oxazoline enabled the optimization of polymer loading by changing only the polymerization time. The adsorption process of lead ions onto POZ-ACs involves complex interactions of lead ions and specific functional groups such as amide moieties in the polymer backbone, ester functionalities of the pendant groups, and electrostatic interactions originated from the aromatic groups that exist on the surface of activated carbon. The Langmuir isotherm and pseudo-second-order kinetic model described the adsorption of lead ions onto the resulting POZ-ACs. This study demonstrated that the adsorbent had a high adsorption capacity of 365 mg/g achieved in a relatively short time of 37 min, with excellent reusability potential for up to seven cycles. However, this study showed that the high solubility of polyoxazoline polymers in water could lead to a decrease in adsorption performance after seven adsorption–desorption cycles due to polymer release into the water media. Despite this limitation, this study highlights the potential of

using polyoxazoline polymers in water treatment applications and suggests future research should focus on developing polyoxazoline polymers with less solubility in water while maintaining a high removal performance.

**Author Contributions:** Conceptualization, A.A., M.B., F.M.S., N.E., C.S. and S.S.S.; data curation, F.M.S. and S.S.S.; formal analysis, A.A., M.B. and S.S.S.; funding acquisition, C.S. and S.R.N.; investigation, F.M.S.; methodology, M.B.; project administration, C.S.; resources, N.E. and C.S.; supervision, S.R.N.; validation, S.S.S.; visualization, A.A. and N.E.; writing—original draft, A.A., M.B., F.M.S., N.E. and S.S.S.; writing—review and editing, S.R.N. All authors have read and agreed to the published version of the manuscript.

**Funding:** This research was funded by the Deanship of Scientific Research at King Khalid University under grant number RGP2/174/44.

**Data Availability Statement:** The data that support the findings of this study are available on request from the corresponding author.

**Acknowledgments:** The authors extend their appreciation to the Deanship of Scientific Research at King Khalid University for funding this work through Research Groups Program under grant number RGP2/174/44.

**Conflicts of Interest:** The authors declare no conflict of interest.

## References

1. Mousazadeh, B.; Mohammadi, N.; Khosravi-Nikou, M. Synthesis and characterization of porous activated carbons derived from lotus nut and their performance for CO<sub>2</sub> adsorption. *Int. J. Environ. Sci. Technol.* **2024**, 1–16. [[CrossRef](#)]
2. Liu, W.; Huang, F.; Liao, Y.; Zhang, J.; Ren, G.; Zhuang, Z.; Zhen, J.; Lin, Z.; Wang, C. Treatment of CrVI-containing Mg(OH)<sub>2</sub> nanowaste. *Angew. Chem.* **2008**, *120*, 5701–5704. [[CrossRef](#)]
3. Basak, S.; Dey, B.; Bhattacharyya, B. Demand side management for solving environment constrained economic dispatch of a microgrid system using hybrid MGWOSCACSA algorithm. *CAAI Trans. Intell. Technol.* **2022**, *7*, 256–267. [[CrossRef](#)]
4. Liu, Z.; Xu, Z.; Zhu, X.; Yin, L.; Yin, Z.; Li, X.; Zheng, W. Calculation of carbon emissions in wastewater treatment and its neutralization measures: A review. *Sci. Total Environ.* **2023**, *912*, 169356. [[CrossRef](#)] [[PubMed](#)]
5. Mousazadeh, B.; Mohammadi, N.; Hamoule, T. Phosphate removal from aqueous environment using iron oxide/activated carbon composite: Ziziphus nuts derived activated carbon as a new precursor. *Iran. J. Chem. Eng. (IJChE)* **2021**, *18*. [[CrossRef](#)]
6. LeChevallier, M.W.; Mansfield, T.J.; Gibson, J.M. Protecting wastewater workers from disease risks: Personal protective equipment guidelines. *Water Environ. Res.* **2020**, *92*, 524–533. [[CrossRef](#)]
7. Chen, D.; Wang, Q.; Li, Y.; Li, Y.; Zhou, H.; Fan, Y. A general linear free energy relationship for predicting partition coefficients of neutral organic compounds. *Chemosphere* **2020**, *247*, 125869. [[CrossRef](#)]
8. Shafqat, S.; Majeed, H.; Javaid, Q.; Ahmad, H.F. Standard ner tagging scheme for big data healthcare analytics built on unified medical corpora. *J. Artif. Intell. Technol.* **2022**, *2*, 152–157. [[CrossRef](#)]
9. Hua, M.; Zhang, S.; Pan, B.; Zhang, W.; Lv, L.; Zhang, Q. Heavy metal removal from water/wastewater by nanosized metal oxides: A review. *J. Hazard. Mater.* **2012**, *211*, 317–331. [[CrossRef](#)]
10. Liu, X. Real-world data for the drug development in the digital era. *J. Artif. Intell. Technol.* **2022**, *2*, 42–46. [[CrossRef](#)]
11. Abdullayeva, F.J. Internet of Things-based healthcare system on patient demographic data in Health 4.0. *CAAI Trans. Intell. Technol.* **2022**, *7*, 644–657. [[CrossRef](#)]
12. Wołowicz, M.; Komorowska-Kaufman, M.; Pruss, A.; Rzepa, G.; Bajda, T. Removal of heavy metals and metalloids from water using drinking water treatment residuals as adsorbents: A review. *Minerals* **2019**, *9*, 487. [[CrossRef](#)]
13. Hamoule, T.; Mohammadi, N.; Mousazadeh, B.; Fakhari, H. Simultaneous improvement of water stability and performance of HKUST-1 for fast cadmium removal from the water environment: Synthesis, characterization, RSM optimization, thermodynamics and kinetics. *Int. J. Environ. Sci. Technol.* **2023**, *20*, 11913–11930. [[CrossRef](#)]
14. Fu, F.; Wang, Q. Removal of heavy metal ions from wastewaters: A review. *J. Environ. Manag.* **2011**, *92*, 407–418. [[CrossRef](#)] [[PubMed](#)]
15. Anwar, J.; Shafique, U.; Salman, M.; Dar, A.; Anwar, S. Removal of Pb (II) and Cd (II) from water by adsorption on peels of banana. *Bioresour. Technol.* **2010**, *101*, 1752–1755. [[CrossRef](#)] [[PubMed](#)]
16. Ahamed, M.; Siddiqui, M. Low level lead exposure and oxidative stress: Current opinions. *Clin. Chim. Acta* **2007**, *383*, 57–64. [[CrossRef](#)] [[PubMed](#)]
17. Şölener, M.; Tunali, S.; Özcan, A.S.; Özcan, A.; Gedikbey, T. Adsorption characteristics of lead (II) ions onto the clay/poly (methoxyethyl) acrylamide (PMEA) composite from aqueous solutions. *Desalination* **2008**, *223*, 308–322. [[CrossRef](#)]
18. Yi, T.; Shi, M.; Zhu, H. Medical data publishing based on average distribution and clustering. *CAAI Trans. Intell. Technol.* **2022**, *7*, 381–394. [[CrossRef](#)]

19. Awual, M.R. An efficient composite material for selective lead (II) monitoring and removal from wastewater. *J. Environ. Chem. Eng.* **2019**, *7*, 103087. [[CrossRef](#)]
20. Kadirvelu, K.; Namasivayam, C. Agricultural by-product as metal adsorbent: Sorption of lead (II) from aqueous solution onto coirpith carbon. *Environ. Technol.* **2000**, *21*, 1091–1097. [[CrossRef](#)]
21. Bandehali, S.; Parvizian, F.; Moghadassi, A.; Hosseini, S.; Shen, J. Fabrication of thin film-PEI nanofiltration membrane with promoted separation performances: Cr, Pb and Cu ions removal from water. *J. Polym. Res.* **2020**, *27*, 94. [[CrossRef](#)]
22. Deng, X.; Lü, L.; Li, H.; Luo, F. The adsorption properties of Pb (II) and Cd (II) on functionalized graphene prepared by electrolysis method. *J. Hazard. Mater.* **2010**, *183*, 923–930. [[CrossRef](#)]
23. Pang, F.M.; Kumar, P.; Teng, T.T.; Omar, A.M.; Wasewar, K.L. Removal of lead, zinc and iron by coagulation–flocculation. *J. Taiwan Inst. Chem. Eng.* **2011**, *42*, 809–815. [[CrossRef](#)]
24. Feng, J.; Yang, Z.; Zeng, G.; Huang, J.; Xu, H.; Zhang, Y.; Wei, S.; Wang, L. The adsorption behavior and mechanism investigation of Pb (II) removal by flocculation using microbial flocculant GA1. *Bioresour. Technol.* **2013**, *148*, 414–421. [[CrossRef](#)] [[PubMed](#)]
25. Xie, H.; Yao, X.; Yu, X.; Mao, L.; Zeng, Y.; Wu, F.; Guo, S.; He, G. Flotation Performance and Adsorption Mechanism of Cerussite with Phenylpropenyl Hydroxamic Acid Collector. *Minerals* **2023**, *13*, 1315. [[CrossRef](#)]
26. Yu, X.; Mao, L.; Xie, H.; Yao, X.; He, G.; Huang, Z. Flotation Behavior and Adsorption Mechanism of Phenylpropyl Hydroxamic Acid As Collector Agent in Separation of Fluorite from Calcite. *Langmuir* **2023**, *39*, 5936–5943. [[CrossRef](#)]
27. Karnib, M.; Kabbani, A.; Holail, H.; Olama, Z. Heavy metals removal using activated carbon, silica and silica activated carbon composite. *Energy Procedia* **2014**, *50*, 113–120. [[CrossRef](#)]
28. Yuna, Z. Review of the natural, modified, and synthetic zeolites for heavy metals removal from wastewater. *Environ. Eng. Sci.* **2016**, *33*, 443–454. [[CrossRef](#)]
29. Li, Z.; Chen, Y.; Wang, Z.; Zhao, Y.; Xia, Q.; Qiu, J.; Wang, H.; Wang, J. Ionic liquid hybrid metal–organic frameworks for efficient adsorption and selective separation of ammonia at high temperature. *Chem. Eng. J.* **2023**, *464*, 142728. [[CrossRef](#)]
30. Mohammadi, N.; Mousazadeh, B.; Hamoule, T. Synthesis and characterization of NH<sub>2</sub>-SiO<sub>2</sub>@Cu-MOF as a high-performance adsorbent for Pb ion removal from water environment. *Environ. Dev. Sustain.* **2021**, *23*, 1688–1705. [[CrossRef](#)]
31. Zheng, X.; Ni, C.; Xiao, W.; Liang, Y.; Li, Y. Ionic liquid grafted polyethersulfone nanofibrous membrane as recyclable adsorbent with simultaneous dye, heavy metal removal and antibacterial property. *Chem. Eng. J.* **2022**, *428*, 132111. [[CrossRef](#)]
32. Ragheb, E.; Shamsipur, M.; Jalali, F.; Mousavi, F. Modified magnetic-metal organic framework as a green and efficient adsorbent for removal of heavy metals. *J. Environ. Chem. Eng.* **2022**, *10*, 107297. [[CrossRef](#)]
33. Viegas, T.X.; Bentley, M.D.; Harris, J.M.; Fang, Z.; Yoon, K.; Dizman, B.; Weimer, R.; Mero, A.; Pasut, G.; Veronese, F.M. Polyoxazoline: Chemistry, properties, and applications in drug delivery. *Bioconjugate Chem.* **2011**, *22*, 976–986. [[CrossRef](#)] [[PubMed](#)]
34. Aoi, K.; Okada, M. Polymerization of oxazolines. *Prog. Polym. Sci.* **1996**, *21*, 151–208. [[CrossRef](#)]
35. Simon, L.; Marcotte, N.; Devoisselle, J.; Begu, S.; Lapinte, V. Recent advances and prospects in nano drug delivery systems using lipopolyoxazolines. *Int. J. Pharm.* **2020**, *585*, 119536. [[CrossRef](#)] [[PubMed](#)]
36. Mahand, S.N.; Aliakbarzadeh, S.; Moghaddam, A.; Moghaddam, A.S.; Kruppke, B.; Nasrollahzadeh, M.; Khonakdar, H.A. Polyoxazoline: A review article from polymerization to smart behaviors and biomedical applications. *Eur. Polym. J.* **2022**, *178*, 111484. [[CrossRef](#)]
37. Sahin, Z.M.; Kohlan, T.B.; Atespare, A.E.; Yildiz, M.; Unal, S.; Dizman, B. Polyoxazoline-modified graphene oxides with improved water and epoxy resin dispersibility and stability towards composite applications. *J. Appl. Polym. Sci.* **2022**, *139*, e52406. [[CrossRef](#)]
38. Portier, É.; Azemar, F.; Benkhaled, B.T.; Bardeau, J.-F.; Faÿ, F.; Réhel, K.; Lapinte, V.; Linossier, I. Poly (oxazoline) for the design of amphiphilic silicone coatings. *Prog. Org. Coat.* **2021**, *153*, 106116. [[CrossRef](#)]
39. Cegłowski, M.; Marien, Y.W.; Smeets, S.; De Smet, L.; D’hooge, D.R.; Schroeder, G.; Hoogenboom, R. Molecularly Imprinted Polymers with Enhanced Selectivity Based on 4-(Aminomethyl) pyridine-Functionalized Poly (2-oxazoline) s for Detecting Hazardous Herbicide Contaminants. *Chem. Mater.* **2021**, *34*, 84–96. [[CrossRef](#)]
40. Soleimani, M.; Abdaliousan, A.; Manshad, A.K.; Sajadiyan, V.A. Advanced polymer-based surfactant for improved heat and salinity stability in enhanced oil recovery processes. *J. Surfactants Deterg.* **2024**. [[CrossRef](#)]
41. Soleimani, M.; Abdaliousan, A.; KhaksarManshad, A.; Sajadiyan, V.A. Synthesis, characterization, and mechanistic study of a new highly-stable comb-like polymeric surfactant in enhanced oil recovery. *Geoenergy Sci. Eng.* **2024**, *234*, 212542. [[CrossRef](#)]
42. Yao, X.; Yu, X.; Wang, L.; Zeng, Y.; Mao, L.; Liu, S.; Xie, H.; He, G.; Huang, Z.; Liu, Z. Preparation of cinnamic hydroxamic acid collector and study on flotation characteristics and mechanism of scheelite. *Int. J. Min. Sci. Technol.* **2023**, *33*, 773–781. [[CrossRef](#)]
43. Soleimani, M.; Abdaliousan, A.; Khaksar Manshad, A.; Sajadiyan, V.A. Polymeric Surfactant Flooding for Improved Oil Recovery: Optimized Wettability and Fluid Mobility. *Iran. J. Chem. Chem. Eng.* **2023**, *in press*.
44. Bouten, P.J.; Lava, K.; van Hest, J.C.; Hoogenboom, R. Thermal properties of methyl ester-containing poly(2-oxazoline)s. *Polymers* **2015**, *7*, 1998–2008. [[CrossRef](#)]
45. Prakash, M.O.; Raghavendra, G.; Ojha, S.; Panchal, M. Characterization of porous activated carbon prepared from arhar stalks by single step chemical activation method. *Mater. Today Proc.* **2021**, *39*, 1476–1481. [[CrossRef](#)]
46. Nayak, S. Water purification: Removal of Heavy metals Using Metal-Organic Frameworks (MOFs). In *Metal-Organic Frameworks in Biomedical and Environmental Field*; Springer: Cham, Switzerland, 2021; pp. 239–268.

47. Wu, Y.; Xu, G.; Liu, W.; Yang, J.; Wei, F.; Li, L.; Zhang, W.; Hu, Q. Postsynthetic modification of copper terephthalate metal-organic frameworks and their new application in preparation of samples containing heavy metal ions. *Microporous Mesoporous Mater.* **2015**, *210*, 110–115. [[CrossRef](#)]
48. Saleem, H.; Rafique, U.; Davies, R.P. Investigations on post-synthetically modified UiO-66-NH<sub>2</sub> for the adsorptive removal of heavy metal ions from aqueous solution. *Microporous Mesoporous Mater.* **2016**, *221*, 238–244. [[CrossRef](#)]
49. Wang, C.; Xiong, C.; He, Y.; Yang, C.; Li, X.; Zheng, J.; Wang, S. Facile preparation of magnetic Zr-MOF for adsorption of Pb (II) and Cr (VI) from water: Adsorption characteristics and mechanisms. *Chem. Eng. J.* **2021**, *415*, 128923. [[CrossRef](#)]
50. Luo, X.; Ding, L.; Luo, J. Adsorptive removal of Pb (II) ions from aqueous samples with amino-functionalization of metal-organic frameworks MIL-101 (Cr). *J. Chem. Eng. Data* **2015**, *60*, 1732–1743. [[CrossRef](#)]
51. Singh, S.; Basavaraju, U.; Naik, T.S.K.; Behera, S.K.; Khan, N.A.; Singh, J.; Singh, L.; Ramamurthy, P.C. Graphene oxide-based novel MOF nanohybrid for synergic removal of Pb (II) ions from aqueous solutions: Simulation and adsorption studies. *Environ. Res.* **2023**, *216*, 114750. [[CrossRef](#)]
52. Huang, Z.; Xiong, C.; Ying, L.; Wang, W.; Wang, S.; Ding, J.; Lu, J. Facile synthesis of a MOF-derived magnetic CoAl-LDH@chitosan composite for Pb (II) and Cr (VI) adsorption. *Chem. Eng. J.* **2022**, *449*, 137722. [[CrossRef](#)]
53. Soltani, R.; Pelalak, R.; Pishnamazi, M.; Marjani, A.; Albadarin, A.B.; Sarkar, S.M.; Shirazian, S. A novel and facile green synthesis method to prepare LDH/MOF nanocomposite for removal of Cd (II) and Pb (II). *Sci. Rep.* **2021**, *11*, 1609. [[CrossRef](#)]
54. Ozdes, D.; Duran, C.; Senturk, H.B. Adsorptive removal of Cd (II) and Pb (II) ions from aqueous solutions by using Turkish illitic clay. *J. Environ. Manag.* **2011**, *92*, 3082–3090. [[CrossRef](#)] [[PubMed](#)]
55. Gundogdu, A.; Ozdes, D.; Duran, C.; Bulut, V.N.; Soylak, M.; Senturk, H.B. Biosorption of Pb (II) ions from aqueous solution by pine bark (*Pinus brutia* Ten.). *Chem. Eng. J.* **2009**, *153*, 62–69. [[CrossRef](#)]

**Disclaimer/Publisher’s Note:** The statements, opinions and data contained in all publications are solely those of the individual author(s) and contributor(s) and not of MDPI and/or the editor(s). MDPI and/or the editor(s) disclaim responsibility for any injury to people or property resulting from any ideas, methods, instructions or products referred to in the content.